Pendent Sulfonylimide Ionic Liquid Monomers and Ionoelastomers via SuFEx Click Chemistry

Authors: Owen A. Lee [1], Matthew K. McBride [2], Matthew Ticknor [1], Joshua Sharpes [2], Ryan C. Hayward [1,2]

[1] Materials Science and Engineering, University of Colorado Boulder, 4001 Discovery Drive, Boulder, CO 80303, USA.

[2] Department of Chemical and Biological Engineering, University of Colorado Boulder, 3415 Colorado Ave, Boulder, CO 80303, USA.

Keywords: Electrolytes, Polymerized Ionic Liquids, Ionic Conductivity, Elastomers, Monomers

Abstract

Anionic polymerized ionic liquids (PILs) with a fixed sulfonylimide group have emerged as promising materials for energy storage applications, electromechanical devices, and gas separation membranes due to their highly delocalized anionic charges. However, synthetic challenges have limited the production of high-purity poly(sulfonylimide)s at scale and hindered systematic evaluation of their properties. We report a synthetic route for the production of high-purity sulfonylimide monomers at > 10 g scales using a Sulfur(VI) Fluoride Exchange (SuFEx) click reaction. Pendent sulfonylimide acrylate monomers with 1-ethyl-3-methylimidazolium counterions were synthesized with perfluorinated side groups of different lengths and crosslinked to form ionoelastomers. The networks were stretchable (≈ 120% strain at break), showed high solvent-free ionic conductivity (> 3.8 x 10^{-3} mS/cm), and were hydrophobic with water contact angles > 105°. The imidazolium counterions interact strongly with the perfluorinated side chains, yielding non-monotonic trends in ionic conductivity and modulus relative to glass transition temperature (T_g). Wide angle X-ray scattering (WAXS) and vibrational spectroscopies reveal that shorter perfluorinated side groups promote cation dissociation, while longer chains cause ionic aggregation. We expect that this SuFEx approach will expand access to next-generation poly(sulfonylimide) electrolytes for a variety of applications, and here demonstrate its utility for providing new insight into the molecular-level design of poly(sulfonylimide) ionoelastomers.

1. Introduction

Polymerized ionic liquids (PILs) consisting of one or more loosely coordinating ions covalently linked to a polymeric backbone have gained significant attention over the last decade for their high solvent-free ionic conductivities under ambient conditions and wide electrochemical windows [1]–[3]. These properties have enabled PILs to be employed in various electronic applications ranging from energy storage devices, such as batteries and supercapacitors, to electromechanical devices such as low-voltage electroadhesives and actuators [4]–[7]. Furthermore, the high degree of chemical diversity among PILs allows for applications-driven polymer design without the constraints associated with other ion-conducting polymer systems, such as the need for solvent or specific ion-backbone interactions.

A wide range of approaches have been developed to synthesize diverse PILs. Particularly, PILs with pendent charges have become popular because they allow for the use of well-established polymerization chemistries, with charged functionalities added pre- or post-polymerization. The decoupling of polymer and fixed ion chemistries affords pendent PILs a high degree of customizability of backbone and IL properties while also allowing for copolymerization with various charged, uncharged, or crosslinkable species [5], [8]–[10].

To date, the majority of pendent PILs have been polycationic, typically with a quaternized ammonium, pyridinium, pyrrolidium, imidazolium, or phosphonium fixed ion and a bulky anionic counterion such as bis(trifluoromethanesulfonyl)imide (TFSI). This chemical diversity has allowed researchers to systematically tune cationic PIL physical properties such as hydrophilicity, modulus, and ionic conductivity by adjusting fixed ion chemistry [1], [2]. In contrast, the choices for polyanionic PILs are much more limited. The most readily available anionic PILs consist of acrylic acid or sulfonate ions covalently linked to the polymer backbone. Acrylic acid and

sulfonate ions have a more localized charge than other weakly associating anions, meaning that polymers containing these species typically exhibit greater hydrophilicity, higher glass transition temperatures (T_g), and lower solvent-free ion conductivity [11].

Macromolecules containing covalently linked sulfonylimide anions are of particular interest as polyanionic PILs due to their more delocalized negative charge. Shaplov, et al. pioneered sulfonylimide PIL synthesis by converting a monomeric sulfonate ion to a sulfonylimide ion through a sulfonylchloride intermediate [11], [12] (Figure 1a), allowing for the incorporation of sulfonylimide groups directly onto polymerizable vinyl [13], (meth)acrylate [6], [12], [14]–[18], and stryrenic handles [19]–[23]. This synthetic approach has been adopted more recently for single alkali-ion conducting polyelectrolytes [13]–[17], [19]–[21], [23]–[27], ion-mediated transistors [28], and CO_2 separations membranes [29], [30]. Sulfonylimide-derived PILs tend to have higher ionic conductivity values and lower glass transition temperatures than their analogous sulfonate counterparts [14], [16], [31], [32]. Moreover, their hydrophobicity makes sulfonylimide PILs relatively insensitive to changes in environmental humidity, a trait desirable for electronics used in ambient conditions [12]. Despite their promise, the existing method to prepare such monomers requires an inert atmosphere and leads to the presence of undesired side products that limit yields and reduce monomer purities. These synthetic challenges have limited the production of poly(sulfonylimide) PILs at scale and hindered systematic evaluation of their electronic and mechanical properties.

Herein, we have developed an alternative route to synthesize these materials using Sulfur (VI) Fluoride Exchange (SuFEx) click chemistry to produce sulfonylimide monomers from their parent sulfonate monomers. SuFEx click chemistry has recently received significant attention as a robust approach for quantitative synthesis of small molecule and polymeric sulfonates and

sulfonamides under moderate conditions, with high purity and yields [33], [34]. Similarly, our approach to pendent sulfonylimide synthesis shows lower sensitivity to air and moisture and yields highly pure ionic liquid (IL) monomers at large scales (~10 g). Although we have recently exploited sulfonylimide monomers prepared using this route in electroadhesive applications [35], we have not previously described the method in detail, nor its extension to other monomers.

Pendent sulfonylimide acrylate monomers were synthesized with perfluorinated side groups of different lengths (1-4 carbons) and 1-ethyl-3-methylimidazolium ($[EMIM]^+$) counterions. Monomers were then photopolymerized with a small amount (2 mol%) of poly(ethylene glycol)diacrylate to produce loosely crosslinked ionoelastomer networks. The resulting networks are stretchable (≈ 120% strain at break), show high solvent-free ionic conductivity (> 3.8 x 10^{-3} mS/cm), and are hydrophobic with water contact angles > 105°. Interestingly, we observe a non-monotonic trend in ionic conductivity and elastic and shear moduli with respect to the glass transition temperature of the ionoelastomer networks. Wide angle X-ray scattering (WAXS) and vibrational spectroscopies reveal this trend to be a balancing act of ionic association and aggregation. Short perfluorinated side groups increase counter-ion dissociation while limiting interactions with the polymer matrix, increasing ionic conductivity. Longer perfluorinated side chains increase ionic aggregation, resulting in a steep reduction in ionic conductivity and an increase in modulus. These findings provide a framework for the design of poly(sulfonylimide) PILs and underscore SuFEx click chemistry as a facile synthetic tool for the fabrication of a variety of poly(sulfonylimide) single-ion conductors.

2. Experimental

2.1 Materials

Potassium 3-sulfopropyl acrylate (KSPA), butylated hydroxytoluene (BHT), poly(ethylene glycol) diacrylate (PEGDA, M_n = 250 g/mol), phenylbis(2,4,6-trimethylbenzoyl)phosphine oxide (I-819), and all solvents were purchased from Sigma and used as received. Oxalyl chloride, sodium chloride (NaCl), potassium bifluoride (KHF_2), sodium sulfate (Na_2SO_3), potassium carbonate (K_2CO_3), and calcium carbonate ($CaCO_3$) were all purchased from Fisher and used as received. Trifluormethanesulfonamide (25 g, >98.0%, TCI), pentafluoroethanesulfonamide (5 g, 99.9%, Ambeed), perfluorobutanesulfonamide (25 g, 98%, 1PlusChem), and 1-ethyl-3-methylimidazolium chloride ([EMIM][Cl], 99.5%, Iolitec Inc) were all used as received without further purification.

2.2 Pendent Sulfonylimide Monomer Synthesis

2.2.1 Synthesis of 3-propylsulfonylchloride acrylate

The synthesis of 3-propylsulfonylchloride acrylate was conducted as described previously [15]. Anhydrous dichloromethane (DCM) (120 mL) was charged in a flame-dried two-opening Schlenk flask. The flask was purged with nitrogen gas (N_2). The DCM was cooled to 0 ^oC and a catalytic amount of dimethylformamide (DMF) (2 mL) was added dropwise. Oxalyl chloride (1.3 EQ, 9.5 mL) was added slowly to the reaction mixture. The mixture was brought to room temperature and stirred for 30 min to form the chlorinating reagent. The flask was again cooled to 0 ^oC and KSPA (1 EQ, 20 g) was slowly added along with 100 ppm BHT (10 mg) as an inhibitor. The reaction proceeded at room temperature overnight in the dark. Water was added to the flask to quench the reaction. The DCM layer was separated and washed with water at least five times.

The organic layer was then washed with saturated NaCl solution (brine) two times and dried for 15 min with sodium sulfate. The DCM was then removed by rotary evaporation and dried under a high vacuum for 15 min. The product 3-propylsulfonylchloride acrylate was a transparent, dark yellow oil, and 16.94 g was recovered (yield: 93% by mole).

2.2.2 Synthesis of 3-propylsulfonylfluoride acrylate

Conversion of (3-propylsulfonylchloride) acrylate to (3-propylsulfonylfluoride) acrylate was carried out as follows. KHF_2 (2 EQ, 12.4 g) was dissolved in water at its solubility limit (0.392 g/mL) in a plastic reaction vessel. The sulfonyl chloride was then dissolved in acetonitrile (AN) (79.5 mL) to form a 1 M solution. The AN solution was added to the KHF_2 solution, and the reaction was allowed to proceed for 4 hr at room temperature. After the reaction, DCM and water were added to the reaction flask and the organic layer was drawn from the aqueous phase. HF is a byproduct of this reaction, so the separated aqueous phase was handled using plastic vessels and was immediately diluted and neutralized with calcium carbonate. The DCM phase was then washed with water five times and then washed two times with brine. The organic layer was then dried for 15 min with sodium sulfate. The DCM was then removed by rotary evaporation. The product (15.25 g, 98% yield) was a clear, light-yellow oil (Figure S1-S2).

2.2.4. Synthesis of 1-ethyl-3-methylimidazolium 3-acryloxypropylsulfonyl(-R-[sulfonimide]) (EA-x) monomers via SuFEx click chemistry

The sulfonylfluoride monomer was used in a sulfur (VI) fluoride exchange (SuFEx) reaction to form potassium 1–[2–acryloyloxypropyl]-R-sulfonylimide followed by ion exchange to synthesize 1-ethyl-3-methylimidazolium 3-acryloxypropylsulfonyl(-R-[sulfonimide]) (EA-x,

x=0, 2, 4). Here we will report the general synthetic procedure for EA-0, or EA for short, which was employed for all EA-x monomers. Sulfonylfluoride monomer (1.3 EQ) was dissolved in AN (non-anhydrous, 1M, 62 mL), followed by 1 EQ of trifluoromethanesulfonamide (9.3 g). 3 EQ of potassium carbonate (25.8 g) was then added to the flask. In ambient air, the solution was then heated to 65 ^{o}C and refluxed overnight. After the reaction, solids were filtered, and the remaining solution was concentrated via rotary evaporation and recrystallized in DCM. The potassium salt product (19.46 g, 86% yield) was a white powder. The quantitative conversion of the sulfonylfluoride group was determined via ^{1}H NMR (Supporting Information, Figure S3-S4). Next, 10 g (27.62 mmol) of the potassium salt was mixed with 1.05 EQ of [EMIM][Cl] at a concentration of 0.5 M in AN and the ion exchange reaction proceeded for 24 hr in the dark. 10mg of BHT was added as an inhibitor. After ion exchange, solids were removed by cold filtration and AN was removed by rotary evaporation. The resulting oil was redissolved in ≈ 40 mL of DCM and the remaining solids were removed by centrifugation (Eppendorf-5430) at 7800 RPM for 5 min. The supernatant was then washed one time with water and DCM was removed via rotary evaporation. The product, a viscous transparent, slightly yellow oil, was further dried under high vacuum for ≈ 1hr. The final product, EA monomeric IL was recovered at an 84% yield (10.06 g, Figure S5-S6, Figure S11-12).

2.3 Ionoelastomer Fabrication

Ionoelastomers were fabricated as previously reported [4], [8]. The following can be considered general for all EA-x monomers. We weighed 250 mg of EA-x monomer in a glass vial and combined it with 2 mol% PEGDA crosslinker. We prepared a 100 mg/mL stock solution of photoinitiator I-819 in DCM. We added 0.5 mol% initiator (1 mol% for EA-4) and vortexed the

vial until thoroughly mixed. We left the solution under vacuum overnight at 22 ºC to remove excess DCM and degas the pre-polymer resin. Molds were prepared by clamping two fluorinated glass slides (Supporting Information) together, separated by 250 μm Teflon spacers (McMaster Carr). The pre-polymer resin was allowed to enter the mold utilizing capillary action. Filled molds were photopolymerized using a UV curing lamp (Melodie Suzie 30 W, 365 nm) for 30 min. Ionoelastomers were then carefully demolded and the sol fraction was removed by soaking in 10 mL of DCM for 24 hr, followed by rinsing with fresh isopropanol (IPA). Residual solvent was removed by heating the films at 60 ºC *in vacuo* for either 24 hr or 1 week. The resulting films were flexible, clear, and could be cut into any testing geometry with ease.

2.4 Spectroscopic and Thermal Characterization

^{1}H-NMR and ^{19}F-NMR spectra were recorded using a Bruker 400 MHz spectrometer with d3-acetonitrile as the solvent. Transparency measurements were performed using an Ocean Optics DH-2000-BAL UV-vis spectrometer. Attenuated total reflection Fourier transform infrared (ATR-FTIR) spectra were collected using a Thermo Scientific iS50 ATR-FTIR spectrometer from 540 cm^{-1} to 4000 cm^{-1}. Raman spectra were collected with a Horiba LabRAM HR Evolution Raman Spectrometer with a 532 nm excitation laser. Raman scans were collected at 50x magnification and an 1800 mm grating with a 30 s collection time per scam. For each material, 12 scans were averaged and the fluorescence signal was subtracted to yield the finished spectrum. DSC thermograms were obtained using a DSC 2500 (TA Instruments) from -80 ºC to 25 ºC at a ramp rate of 10 ºC/min. Glass transition temperatures were determined from the 2nd heating cycle.

2.5 Mechanical Characterization

Tensile tests were conducted using a DMA 850 (TA Instruments) mechanical tester. Samples were cut into 0.5 cm x 2 cm rectangles and stretched at a strain rate of 5 %/min at a temperature of 22 °C. Young's moduli were determined using the slope of the stress-strain curve from 1-3 % strain. Rheology measurements were conducted using ARES G2 rheometer with an 8mm Teflon probe. Rheology frequency sweeps were conducted from 0.1 Hz to 50 Hz.

2.6 Ionic Conductivity Measurements

The ionic conductivity was measured using a Gamry 600+ potentiostat with an Instec STC200 temperature controller. The samples were prepared by sandwiching 0.5 cm diameter circular EA-x films between ITO-coated glass slides with Teflon spacers. Transparent ITO electrodes were used to ensure conformal contact between the ionoelastomer and electrode surface, while also allowing for in-situ determination of sample area and thickness *in situ*. AC potentials of 40 mV were applied in the frequency range of 1 MHz to 0.1 Hz. The conductivity was calculated using equation (1):

$$\sigma_{DC} = \frac{L}{R_{DC}A} \quad \text{(EQ 1)}$$

where R_{DC} is the mid-frequency plateau of the impedance modulus, L is the sample thickness, and A is the sample area. Temperature-dependent conductivity measurements were conducted from 60 °C to 15 °C in 5 °C increments. A 20 min delay time was added once a steady state temperature was reached to ensure a uniform temperature profile across the thickness of the sample.

2.7 X-Ray Scattering

Wide angle X-ray scattering (WAXS) was conducted using Xenox Xeus 3.0 WAXS system with a 50 kV Cu Ka X-ray source in the standard configuration. Samples were loaded in transmission at < 0.4 mBar vacuum with a sample-to-detector distance of 48.5 mm. Background subtracted 2D patterns were integrated azimuthally to yield 1D curves using XSACT software.

2.8 Contact angle Goniometry

Water contact angles EA-x ionoelastomer films were measured using a custom-built pendant drop tensiometer and with MilliQ water (< 18.2 MΩ cm). Static contact angle measurements were taken 5 s after a 1 μL drop was deposited on the surface of the film. Advancing contact angle measurements were taken as the average contact angle as water was added to a droplet over a 2 s interval while receding contact angle measurements were taken as the average contact angle as water was removed from a droplet over a 2 s interval. We analyzed the collected images using First Ten Angstroms contact angle software (FTA32, Portsmouth, VA) employing a sessile drop model.

3. Results and Discussion

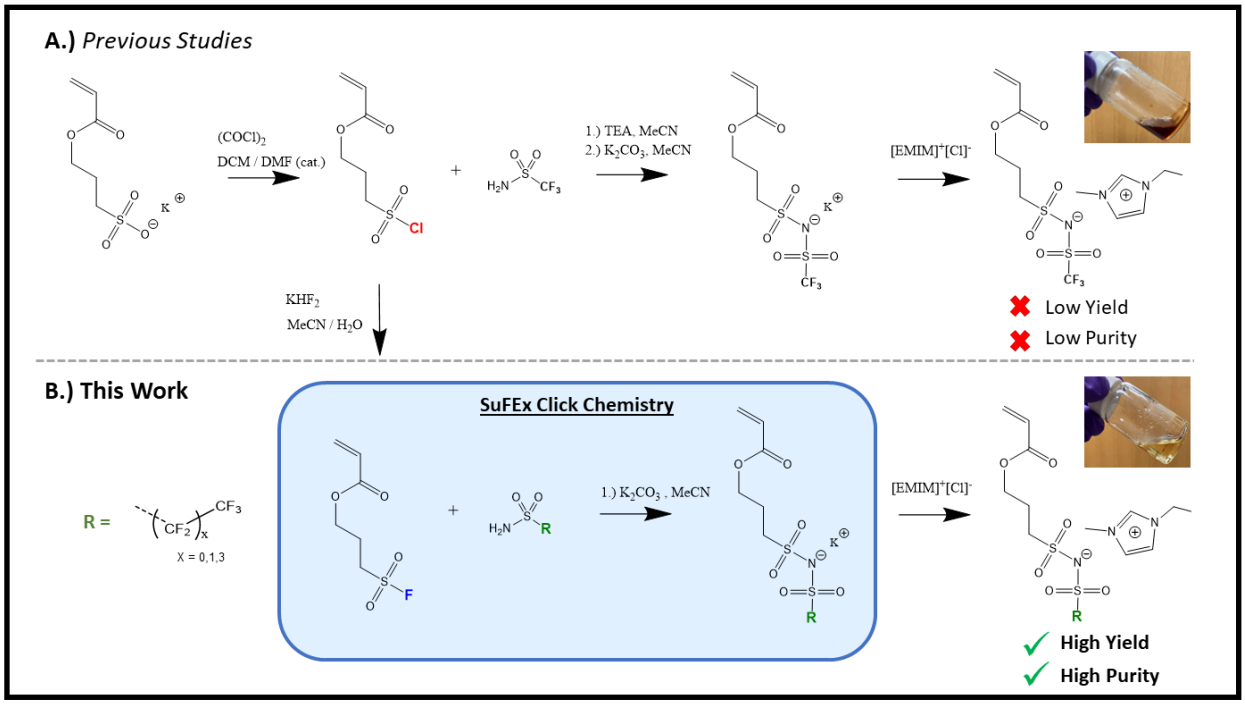

Figure 1: A) Previous synthetic approach to pendent sulfonylimide synthesis using sulfonylchloride intermediate. The sulfonyl chloride reacts with triethylamine (TEA) and a sulfonamide to create a triethylammonium sulfonylimide ionic liquid (IL) intermediate (not pictured). This intermediate can then be reacted with an alkaline base like potassium carbonate (K_2CO_3), to yield an alkaline pendent sulfonylimide salt, which can more easily be ion exchanged. The inset image corresponds to the EA IL monomer synthesized using the conventional approach. **B)** Our approach to pendent sulfonylimide synthesis using SuFEx click chemistry. The sulfonylchloride is converted to a sulfonylfluoride, which can then be clicked onto a sulfonamide to yield an alkaline pendent sulfonylimide salt in a single step, without the IL intermediate. The inset image corresponds to the EA IL monomer synthesized by way of SuFEx click chemistry.

3.1. Monomer Synthesis.

Identical pendent trifluoromethanesulfonylimide acrylate (EA) monomers were synthesized as previously reported [15] (Figure 1A), and with our new SuFEx click approach (Figure 1B). We found that going directly from the sulfonylchloride to the trifluormethanesulfonylimde monomer, resulted in a final product with significant impurities that

we were unable to remove. The resulting ionic liquid (IL) monomer was red-brown in color and translucent; indicative of impurities. We identify two potential sources for these impurities. First, the sulfonylchloride group is easily reduced by nucleophiles, resulting in an unstable R-SO_2^- that can undergo additional side reactions [33]. Second, TEA is prone to oxidative decomposition with prolonged exposure to air, resulting in a yellow to yellow-brown impurity. This process is accelerated in the presence of water, meaning that conversion of the sulfonylchloride must be conducted in air-free, extremely dry conditions for high-purity products [36].

Alternatively, EA monomer synthesized via SuFEx click reaction and subsequent ion exchange was an optically clear liquid and had high purity from ^{1}H NMR, ^{13}C NMR, and ^{19}F NMR (Figure S5-S6, Figure S11-12), despite being synthesized under ambient conditions with non-anhydrous solvents. This is because the SO_2-F bond is less prone to reduction [33], and thus the SuFEx reaction can proceed quantitatively directly to the alkali salt (Figure 1B) without TEA or the triethylammonium intermediate.

The use of efficient SuFEx chemistry enabled the synthesis of a series of pendent sulfonylimide monomers with varying perfluorinated (-CFx) alkyl side chain lengths with similarly high purity (Supporting Information, Figures S7-S12). Poly(sulfonylimide)s with perfluorinated alkyl groups are commonly employed in the literature as analogs of the loosely coordinating TFSI small molecule anion. However, a detailed description of the effect of CF_x terminal chain length on material properties has yet to be reported for linear or crosslinked room-temperature polymerized ionic liquids (PILs), motivating this study. Sulfonylimide monomers with perfluoroalkyl terminal groups of 1, 2, and 4 carbons were chosen as all three monomers could be synthesized following the same synthetic and purification scheme using commercially available perfluoroalkanesulfonamide reagents. All EA-x monomers had a slightly yellow color

(Figure S13), which we attribute to the sacrificial decomposition of the added BHT inhibitor during the work up.

3.2. EA-x Ionoelastomer Design and Characterization

The effect of certain pendant side groups on poly(sulfonylimide) physical and electronic properties have been studied in select publications [37], [25], [31]. However, to our knowledge, there has not been a systematic study on the effect of side groups on poly(sulfonylimide) properties with room-temperature ionic liquid pairs. Here, we take advantage of the ease and versatility of SuFEx click chemistry to synthesize a family of three pendent sulfonylimide ionoelastomers with $[EMIM]^+$ mobile ions where the perfluorinated terminal portion of the pendent sulfonylimide is systematically varied in length from 1 to 4 carbons (Figure 2A).

Ionoelastomers were fabricated as previously described, washed with DCM for 24 hr to remove the sol fraction, and dried *in vacuo* to yield a solvent-free ion conducting membrane with gel fractions >80% (Table S1). ATR-FTIR spectra of the three ionoelastomers do not show a characteristic acrylate peak at ≈ 1630 cm^{-1} (Figure S14-S15), indicating that all residual monomer was reacted or washed out as part of the sol fraction. High-resolution ATR-FTIR spectra were collected for EA-x ionoelastomers in the region of C-H stretches for the imidazolium counter-ion (2800-3500 cm^{-1}, Figure S16). We find that the intensity of all imidazolium C-H stretches decreases with increasing perfluorinated side chain length, consistent with the expected decrease in ion concentration as the length of the pendent groups is increased. EA-x ionoelastomers derived from SuFEx click reaction were optically clear (Figure 2B), a property desirable for many stretchable electronic devices such as artificial skins and flexible optoelectronic devices [38].

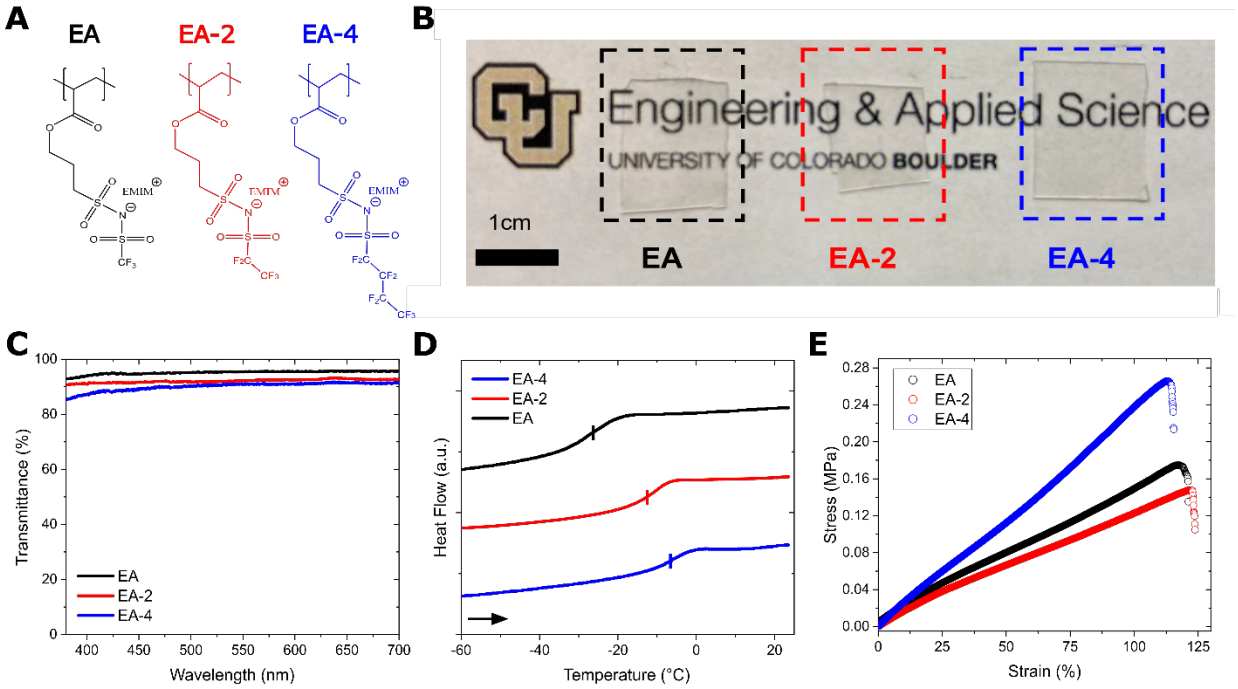

Figure 2: A) The chemical structures of the three ionoelastomers studied in this work. The PEGDA crosslinker was omitted for simplicity. **B)** Optical image of 250 μm thick films of EA, EA-2, and EA-4 ionoelastomers. The image of the bridge is easily seen through transparent ionoelastomer networks. **C)** The transmittance of visible light through 250 μm thick ionoelastomer films. **D.)** DSC thermograms of the second heating cycle for EA-x ionoelastomers with marked glass transition temperature **E.)** Representative stress-strain curves for EA-x ionoelastomers measured using a strain rate of 5 %/ min

All EA-x ionoelastomers had > 90 % transmittance for essentially the entire visible spectrum (Figure 2C). Alternatively, pendent sulfonylimide polymers with monomers synthesized using the conventional method often have a hazy yellow-brown color, despite their non-polymerizable counterparts being clear slightly yellow liquids or white salts [15], [29], [39]–[41].

All EA-x ionoelastomers have a single T_g and do not show additional transitions in the temperature range of -80 ºC to 25 ºC (Figure 2D). Glass transition temperatures increased monotonically with increased perfluorinated side chain length (Table 1) from -26 ºC for EA to -6

°C for EA-4. Moreover, the T_g of EA-x ionoelastomers could readily be tuned by copolymerization of different EA-x monomers. For instance, an ionoelastomer polymerized with 1:1 mole ratio of EA:EA-4 exhibited an intermediate T_g of -11 °C (Figure S17). The increase in T_g with increase perfluorinated terminal group length is consistent with previous studies on ILs and PILs in which the length of perfluorinated side groups of bis(perfluoroalkanesulfonimide) counterions were varied. [42], [43]. We attribute this increase in T_g to strong interactions between the perfluorinated side groups and the imidazolium counter-ion via ion-dipole interactions or hydrogen bonding [9].

The room temperature Young's modulus (Table 1, Figure 2E) was nearly identical for EA (193 ± 28) and EA-2 (175 ± 10 kPa), however, it was nearly 1.5 times greater for EA-4 (264 ± 43 kPa). For unentangled networks well above T_g, we would expect the modulus to be inversely proportional to the average molecular weight between crosslinks. However, for linear PILs, it has been shown that ionic aggregates act as physical linkages, increasing the effective modulus [44]–[46]. Previous studies have also found that increasing the fluorinated side chain length on bis(perfluoroalkylsulfonimide) counterions generally increases the elastic modulus of poly(vinylimidazolium) PILs [47].

Table 1: Physical, mechanical, and electronic properties of EA-x ionoelastomers. Error values indicate the range taken from three separate measurements.

Polymer	DSC T_g (°C)	Density (g/cm^3)	σ_{DC} (22°C) (mS/cm)	Young's Modulus (kPa)	Elongation at Break (%)
EA	-26	1.41	3.2 ± 0.1 x 10^{-3}	193 ± 28	116 ± 16
EA-2	-13	1.45	3.8 ± 0.5 x 10^{-3}	175 ± 10	112 ± 8
EA-4	-6	1.44	4.7 ± 0.6 x 10^{-4}	264 ± 43	120 ± 15

3.5 Ion Conduction in EA-x Ionoelastomers

To evaluate the effect of pendant group length onion transport by sulfonylimide-derived ionoelastomers, we measured the conductivity at room temperature (Table 1) by means of AC impedance spectroscopy (Figure S18). Generally, for polymer electrolytes, lowering the T_g of the material tends to increase ionic conductivity by increasing segmental motion and available free volume for ion conduction. PILs are somewhat unusual in that in some cases ion motion can be decoupled from segmental dynamics, which is thought to be due to the chain packing frustration of charged pendants [48], [49]. Interestingly, EA-2 showed the highest room temperature (22 °C) conductivity of 3.8 x 10^{-3} mS/cm, despite having a higher T_g and lower ionic concentration than EA (σ_{DC} = 3.1 x 10^{-3} mS/cm). These room temperature conductivity values represent a clear improvement (~ 10x) over previously reported imidazolium-conducting ionoelastomers (Table S2). EA-4, however, showed nearly 10x lower room temperature conductivity (4.7 x 10^{-4} mS/cm), which can at least partially be ascribed to its increased T_g compared to EA and EA-2. Copolymerization of EA with EA-4 in a 50 mol% ratio, resulted in a room temperature conductivity roughly half that of EA networks (1.3 ± 0.2 x 10^{-3} mS/cm), indicating that in random EA-x copolymer ionoelastomers, the monomeric unit with higher ionic conductivity dominates ion transport (Figure S19). Normalizing the temperature of each EA-x ionoelastomer by its T_g, we find that EA-2 and EA-4 have higher ionic conductivity (Figure 3B), indicating the perfluorinated terminal group helps increase imidazolium conduction in the limit of equivalent contributions from segmental relaxation.

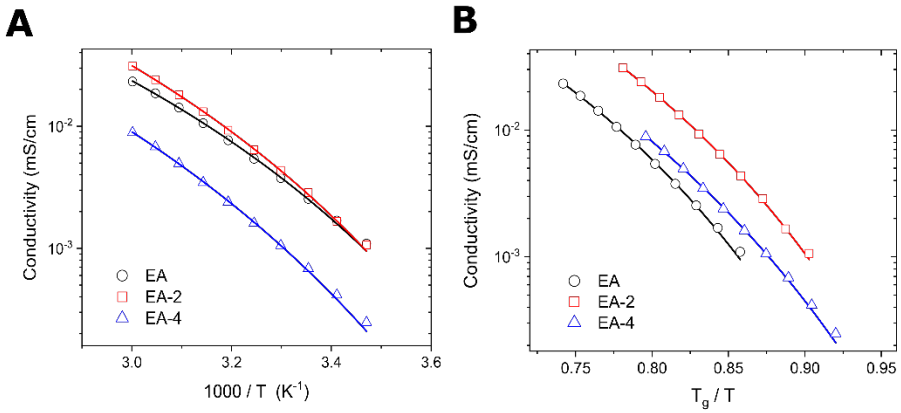

Figure 3: A.) Temperature dependent conductivity of EA-x ionoelastomers as a function of inverse temperature. Lines correspond to the weighted fit of the data (symbols) using EQ. 2. **B.)** Conductivity versus inverse temperature normalized to T_g measured using DSC.

To better understand the molecular origins of this non-monotonic trend in conductivity with respect to the glass transition temperature, we conducted temperature-dependent conductivity measurements (Figure 3a, Figure S20). To ensure that these samples were solvent-free, samples were dried *in vacuo* for 7 days. We find that the results are in excellent agreement with our RT conductivity data. We then fit the data to the Vogel-Fulcher-Tammann (VFT) equation:

$$\sigma_{DC}(T) = \sigma_{\infty} e^{\left(\frac{-B}{T-T_o}\right)} \qquad \text{(EQ 2)}$$

where $\sigma_{DC}(T)$ is the temperature-dependant DC conductivity of the material, σ_{∞} is the conductivity in the limit of infinite temperature, B is a fitting constant related to the activation energy for ion conduction and T_o is the Vogel temperature, which is typically around 50 K below T_g. A summary of the fitted parameters can be found in Table 2.

Table 2: Fitted parameters to the VFT equation (EQ 2) with the measured T_g from DSC for EA-x ionoelastomers. Error corresponds to the standard error of the non-linear fit.

Polymer	σ_∞ (mS/cm)	B	T_o (K)	$T_{g,\,DSC}$ (K)
EA	10 ± 3	790 ± 80	203 ± 6	247
EA-2	21 ± 4	840 ± 50	204 ± 4	260
EA-4	13 ± 6	1000 ± 100	201 ± 7	267

The value of T_o determined by VFT fitting is nearly constant between the three EA-x ionoelastomers, ranging only from 201 - 204 K while the T_g measured by DSC increased by 20 K with increasing fluorinated side chain length from EA to EA-4. However, for PILs, a discrepancy between the effective T_g (T_o + 50 K) derived from the VFT equation, related to conductivity relaxation, and the T_g derived from DSC, related to segmental relaxation, is frequently observed due to the decoupling of ion conduction from segmental dynamics [48]. For EA-x ionoelastomers, increasing the perfluorinated terminal functionality increases this decoupling from segmental dynamics, leading to the observed increase in T_g normalized conductivity for EA-2 and EA-4 compared to EA (Figure 3B). Conversely, the VFT fit indicates a much higher value of the prefactor σ_∞, for EA-2, compared to EA or EA-4. Interestingly, EA-4 also had a higher value of σ_∞ compared to EA. We attribute this increase to the increase in the dissociation of imidazolium by pendent fluorinated side chains. Similar trends have been reported for ammonium PILs with TFSI counterions, in which adding an additional ethylene glycol unit to the pendant structure increased the infinite temperature dielectric relaxation time scale, analogous to σ_∞ in conductivity space [48]. However, this does not account for the decrease in σ_∞ between EA-2 and EA-4, despite an increase in T_g. Here, we note that ion conduction is a product of both ion concentration and ion

mobility. Thus, it is possible that EA-4 has a lower ion mobility than EA-2, resulting in a lower value of σ_∞, which could point toward an increase in aggregation or change in imidazolium coordination state for EA-4 ionoelastomers. This would also be consistent with the higher linear elastic Young's modulus for EA-4 (Table 1). The following sections will attempt to rationalize this non-monotonic trend in ionic conductivity by investing polymer morphology, ionic aggregation, and ionic coordination.

3.8 Enhanced ionic aggregation leads to lower DC conductivity.

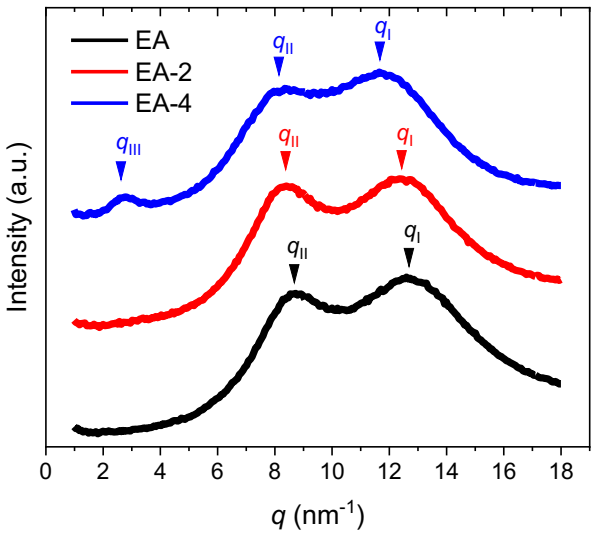

Figure 4: Wide angle X-ray scattering (WAXS) curves for EA-x ionoelastomers. Curves for EA-2 and EA-4 have been shifted vertically for clarity.

Wide angle X-ray scattering was employed to elucidate the underlying mechanism for the observed non-monotonic trend in ionic conductivity by investigating network morphology. WAXS curves were obtained in the range of scattering vector q = 1-18 nm^{-1} (Figure 4). Previous studies on PILs have identified three broad peaks in this range: q_I at > 12 nm^{-1} , the amorphous halo, q_{II}

generally at > 5 nm^{-1} but < 15 nm^{-1}, corresponding to the average counterion spacing, and q_{III} at < 6 nm^{-1} corresponding to the spacing between ionic aggregates [10], [14], [44], [46], [50]–[52].

For EA-x ionoelastomers, we observe three distinct peaks only for EA-4, which shows a clear q_{III} aggregation peak centered at 2.7 nm^{-1}. EA and EA-2 only show q_{II} and q_{I} as distinct peaks. The q_{I} and q_{II} peaks both shift towards lower q (larger spacing), indicating that the longer perfluorinated side chain slightly increases the available space for ion conduction between pendants. The lack of a clear q_{III} peak for EA and EA-2 suggests a smaller degree of aggregation and a broader range of inter-aggregate spacing compared to EA-4 [45]. We propose that the substantially decreased ion conductivity of EA-4 compared to EA and EA-2 is due to this increase in ion aggregation. Copolymerization of EA with EA-4 results in a broader and smaller magnitude q_{III} peak at the same position (Figure S21), indicating copolymerization of loosely aggregating components decreases total ionoelastomer aggregation. However, the higher ionic conductivity of EA-2 with respect to glass transition temperature cannot be fully explained using X-ray scattering alone, as neither show peaks corresponding to regular spacing of ionic aggregates.

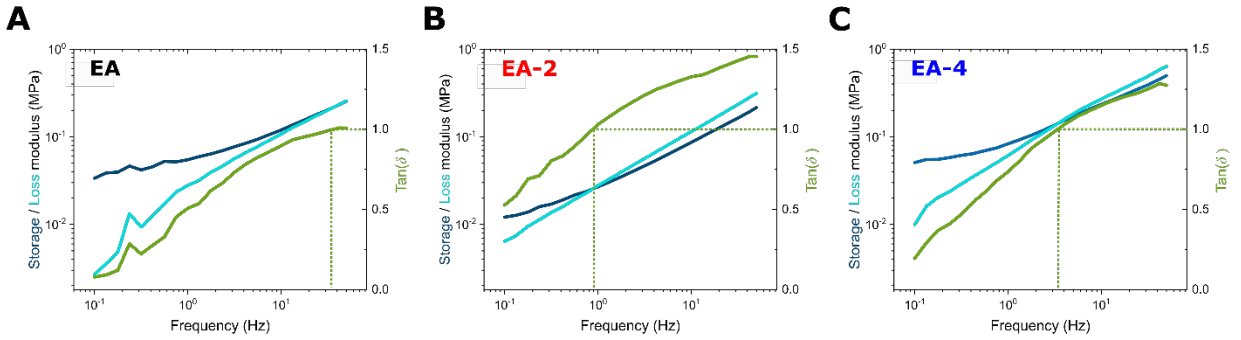

Figure 5: Oscillatory shear rheology measurements of **A.)** EA **B.)** EA-2 and **C.)** EA-4 in the frequency range of 0.5 - 50 Hz at 25 ºC. Dashed red lines indicate the frequency at which the loss modulus exceeds that of the storage modulus (*e.g.* where Tan(δ) = 1)

To help decipher the observed non-monotonic trend in ionic conductivity, oscillatory shear rheology measurements were conducted on EA-x ionoelastomers to further probe ionic aggregation (Figure 5). We found that in small strain frequency sweeps at 25 ^{o}C, there exists a non-monotonic trend in plateau modulus (taken as the modulus at 0.1 Hz) with EA-4 > EA > EA-2, which is in good agreement with the trend in elastic modulus (Table 1). Interestingly, all EA-x ionoelastomers exhibited a crossover frequency where the loss modulus (G") becomes greater than the storage modulus (G') upon increasing frequency between the rubbery plateau at low frequencies and the glass transition at high frequencies. Similar behavior has been found in select charged and uncharged polymers as they approach T_g [46], [43]. Were the crossover to reflect a broad rubbery-to-glass transition, however, we would expect this frequency to decrease with increased polymer T_g. In contrast, for EA-x ionoelastomers, we observe a non-monotonic trend in this crossover frequency, with EA-2 having the lowest crossover frequency, despite having a lower T_g than EA-4.

Alternatively, similar crossover behavior has also been found in entangled polyelectrolyte complex coacervates, with a characteristic frequency corresponding to the exchange rate between neighboring pendent ion pairs [53]. We hypothesize that the crossover event in the ionoelastomers studied here can be explained in part by a similar phenomenon in which ionic aggregates, rather than ionic bonds, act similarly to physical crosslinks between chains. As aggregates break, chains are free to move past one another, resulting in G" exceeding G' well below the frequency associated with T_g. For EA-2, the degree of ion ionic aggregation appears to be lower, resulting in a lower terminal modulus and crossover frequency compared to EA or EA-4.

3.7. Ionic association determines aggregation and conductivity of EA-x ionoelastomers.

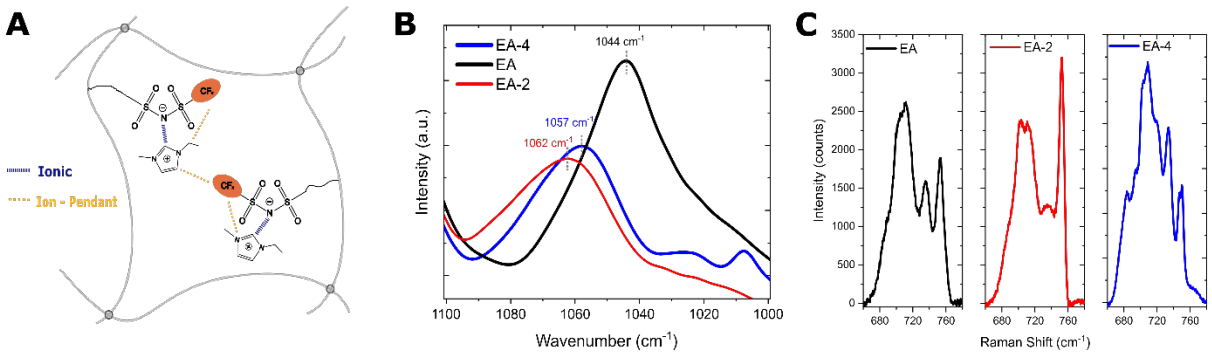

Figure 6: Probing sulfonylimide-imidazolium interactions via vibrational spectroscopies A.) Schematic representation of an EA-x ionoelastomer network including possible ion-ion and ion-pendant interactions with imidazolium counterions B.) AT-FTIR spectra of EA-x ionoelastomers showing the S-N asymmetric band C.) Raman spectra of EA-x ionoelastomers in the region of the SNS breathing mode for EA-x ionoelastomers

Vibrational spectroscopy techniques are commonly employed in both the ionic liquid and single ion conducting polymer communities to provide insight into the degree of ionic association and coordination. For example, spectroscopic evidence of interactions between sulfonylimide and imidazolium can be observed in the S-N (≈ 1050 cm^{-1}) and S=O (≈ 1350 cm^{-1}) asymmetric stretching bands in AT-FTIR spectra. Both bands exhibit a characteristic blue shift when the negative charge is more highly localized on the sulfonylimide nitrogen atom, which has previously been interpreted as reflecting weaker anion-cation associations due to competing ion-dipole interactions between imidazolium and perfluorinated alkyl chains (Figure 6A) [9], [54-57]. Here, we observe such a blue shift of the S-N asymmetric band from 1044 cm^{-1} for EA to 1062 cm^{-1} and 1057 cm^{-1} for EA-2 and EA-4 respectively (Figure 6B). However, the S=O stretching band (Figure S22) does not show the same trend, presumably due to the difference in the electron density of SO_2-CF_2- compared to SO_2-CF_3 The shift in the S-N band indicates a more localized negative charge on the sulfonylimide for EA-2 and EA-4 compared to EA, consistent with stronger cation-

pendant interactions, though we note that the difference in electron withdrawing character of $-CF_3$ vs. $-CF_2-$ pendants may also directly influence the electron density.

Raman spectroscopy can also be employed to probe the local chemical environment of the sulfonylimide unit via measurement of symmetric stretching bands. In lithium-ion conducting poly(sulfonylimide)s this is done by analyzing the SNS breathing mode peaks in the range of 730-760 cm^{-1}. By deconvoluting these peaks, one can quantify the degree of ionic coordination between the counterion and the sulfonylimide anion, with higher wavenumber peaks corresponding to more coordinated binding states [23], [14], [58-60]. Interestingly, for EA-x ionoelastomers, the SNS breathing mode appears as two distinct peaks at ≈ 735 cm^{-1} and ≈ 753 cm^{-1} on the shoulder of a broader peak centered around ≈ 710 cm^{-1}, corresponding to the C=O breathing mode of the acrylate backbone and the $-CF_2-$ stretches for EA-2 and EA-4 (Figure 6C). Interpreting these two SNS breathing mode peaks as two distinct coordination states of pendent sulfonylimide ions, as is the typical interpretation for lithium-ion conducting poly(sulfonylimide)s, we find that the most coordinated state corresponding to the peak at 753 cm^{-1} is most favored for EA-2 compared to EA or EA-4. We hypothesize that the coordination state at 753 cm^{-1} is the singly coordinated state between imidazolium cation and sulfonylimide anion, while the coordination state at 735 cm^{-1} represents ion associations between imidazolium and multiple sulfonylimide ions. We speculate that the more favorable pendant-cation interactions in EA-2, compared to EA, promote the singly-coordinated state which leads to higher RT ion conductivity for EA-2 compared to EA, despite EA-2 having a lower total ion concentration and higher T_g. However, increasing the perfluorinated terminal group to 4 carbons in EA-4 results in an increase in ion aggregation and a return to predominantly multiply-coordinated cations and reducing conductivity. This picture is also consistent with the mechanical and rheological measurements discussed above, which indicate a

lower degree of physical‘crosslinking’ by aggregation and/or multiple coordination of counterions in EA-2 compared to EA and EA-4. Ion conduction in EA-x ionoelastomers can thus be considered a balance of ion association and aggregation, with weak, singly coordinated ions in EA-2 promoting high ionic conductivity values.

3.8. Hydrophobicity of EA-x Ionoelastomers

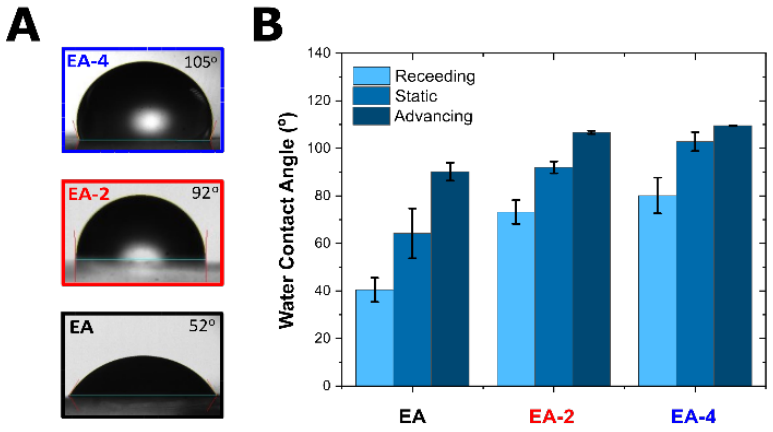

Figure 7: A.) Representative photographs of static water contact angles with EA-x ionoelastomers **B.)** Static, advancing, and receding contact angles for EA-x ionoelastomers, with error bars corresponding to the range of three separate measurements.

Water-resistant ion conductors are useful for real-world applications in which materials are exposed to wet or humid conditions. However, the design of intrinsically hydrophobic ion conductors has been a challenge as most ionic groups are hydrophilic. Poly(sulfonylimide)s have drawn attention for being more hydrophobic than other polyanionic ion conductors, however, a framework for designing hydrophobic poly(sulfonylimide)s has not been reported. As such, we investigated the effect of pendent fluorinated chains on the hydrophobicity of EA-x ionoelastomers. By crosslinking our polymers into free-standing films, we could observe the contact angle of liquid water with the surface of EA-x ionoelastomers (Figure 6a). It was found that the average static contact angle was 64°, 92°, and 105° for EA, EA-2, and EA-4 respectively,

corresponding to a decrease in surface energy and an increase in hydrophobicity with increasing perfluorinated side chain length. Ionoelastomers formed by copolymerization of equal parts EA and EA-4 resulted in networks with an intermediate static water contact angle of 88° (Figure S23). The EA ionoelastomers showed the most contact angle hysteresis with nearly a ≈ 50° difference between advancing and receding contact angles, while EA-2 and EA-4 had less hysteresis (33° and 28° respectively) as shown in Figure 6B. Interestingly, all three homopolymers showed advancing contact angles > 90°, indicating that water does not wet the surface initially, but wettability increases over time. This could be due to surface reorganization, or potentially the small amount of hydrophilic PEGDA, which could provide a route for water to permeate through the surface.

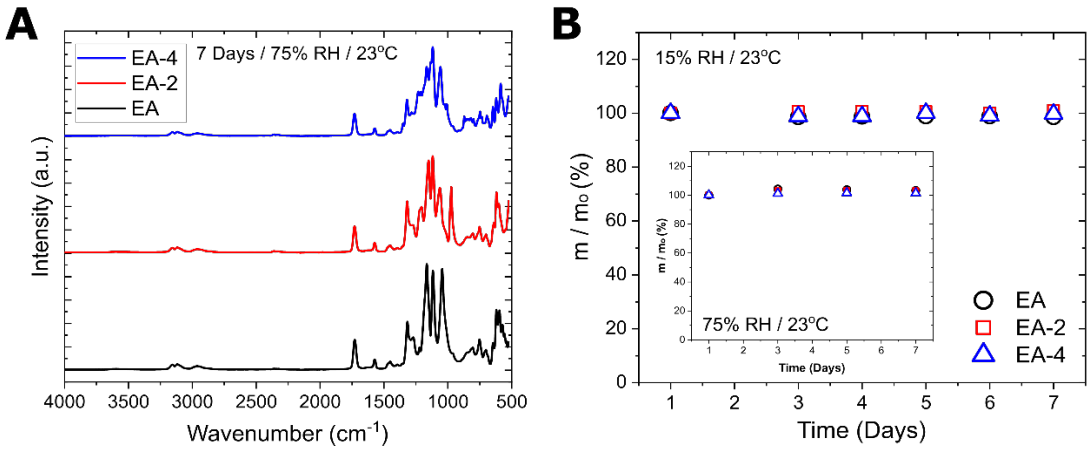

Figure 8: A.) ATR-FTIR spectra of the exposed surface of EA-x ionoelastomers after 7 days at 75% RH. Spectra are vertically shifted for clarity. **B.)** The weight percent of EA-x ionoelastomers as a function of exposure time (days) under ambient conditions (15% RH and 23°) with inset showing the results at 75% RH.

Ionoelastomers were also relatively insensitive to environmental humidity, with no sign of water in the ATR-FTIR spectra of all EA-x ionoelastomers after 7 days under ambient, e.g. 15% relative humidity (RH), and humid, e.g. 75% RH, conditions (Figure 8a, Figure S24). Furthermore, it was

found that the weight of EA-x samples was essentially constant (< ±1 wt%) over a 7-day period at 15% RH. A small increase (≈ 4 wt% and ≈ 3 wt%) was observed for EA and EA-2 samples after 7 days at 75% RH, while EA-4 showed a negligible increase in weight (< 1wt%) in the same period. This is in line with EA-4 also being the most hydrophobic of the EA-x ionoelastomers, but the difference is sufficiently small to also be due to experimental error. EA-x ionoelastomers can thus be considered non-hygroscopic under ambient and humid conditions.

4. Conclusion

We have developed an alternative route to synthesize poly(sulfonylimide) monomers utilizing Sulfur (VI) Fluoride Exchange (SuFEx) click chemistry. This synthetic approach can be conducted under ambient conditions and yields highly pure ionic liquid (IL) monomers at large scales (~10 g). Anionic sulfonylimide ionoelastomers were synthesized with perfluorinated side chains of one, two, and four carbons. These ionoelastomers were stretchable (≈ 120% strain at break), showed high solvent-free ionic conductivity (> 3.8 x 10^{-3} mS/cm), and were hydrophobic with water contact angles > 105° and extremely low sensitivity to humidity.

Our results indicate that conduction of the imidazolium counterions is highly dependent on the perfluorinated side chain length with shorter chains promoting cation dissociation, and longer chains causing ion aggregation. The result is a non-monotonic trend in ion conductivity with respect to T_g with EA-2 having the highest ionic conductivity and lowest modulus, despite having intermediate T_g compared to EA and EA-4. These results, however, probe EA-x ion transport and mechanical properties in a limited temperature and frequency window. Further studies, focusing on separating ion and polymer contributions to conductivity using more complex rheological and AC electronic characterization techniques, would enable more robust statements on the exact

mechanism for ion conduction in EA-x ionoelastomers. In addition, molecular simulations to better understand the role of imidazolium-pendant and sulfonylimide-imidazolium interactions in these materials would be valuable. Furthermore, the ionoelastomers presented in this work cannot be considered model networks, nor have the network structure or chemistry been optimized to enhance ionic conductivity or stretchability. Future work will be required to better assess how ionic associations, crosslinking chemistry, and network inhomogeneities affect ionoelastomer mechanical and electronic properties. We anticipate SuFEx chemistry will provide an enhanced synthetic route for future poly(sulfonylimide) electrolytes for and that our findings give new understanding into the molecular-level design of poly(sulfonylimide) PILs and ionoelastomers.

5. Acknowledgements

This work was supported by the US National Science Foundation through grant DMR-2104892, and made use of an X-ray scattering instrument purchased through ONR DURIP grant number N00014-22-1-2361.

6. Conflicts of Interest

The University of Colorado Boulder has filed a provisional patent application that includes the synthesis of ionic liquid monomers and ionoelastomers using SuFEx chemistry.

7. Supporting Information

The Supporting Information is available free of charge at:

- Experimental details of EA-2 and EA-4 monomer synthesis and characterization (NMR, photographs). Additional EA-x ionoelastomer characterization (ATR-FTIR, Mechanical Characterization, AC Impedance)

8. Works Cited

[1] N. Nishimura and H. Ohno, "15th anniversary of polymerised ionic liquids," *Polymer*, vol. 55, no. 16, pp. 3289–3297, Aug. 2014, doi: 10.1016/j.polymer.2014.02.042.

[2] A. Eftekhari and T. Saito, "Synthesis and properties of polymerized ionic liquids," *Eur. Polym. J.*, vol. 90, pp. 245–272, May 2017, doi: 10.1016/j.eurpolymj.2017.03.033.

[3] J. Yuan, D. Mecerreyes, and M. Antonietti, "Poly(ionic liquid)s: An update," *Prog. Polym. Sci.*, vol. 38, no. 7, pp. 1009–1036, Jul. 2013, doi: 10.1016/j.progpolymsci.2013.04.002.

[4] H. J. Kim *et al.*, "Low-Voltage Reversible Electroadhesion of Ionoelastomer Junctions," *Adv. Mater.*, vol. 32, no. 25, p. 2000600, 2020, doi: 10.1002/adma.202000600.

[5] X. Ming, C. Zhang, J. Cai, H. Zhu, Q. Zhang, and S. Zhu, "Highly Transparent, Stretchable, and Conducting Ionoelastomers Based on Poly(ionic liquid)s," *ACS Appl. Mater. Interfaces*, vol. 13, no. 26, pp. 31102–31110, Jul. 2021, doi: 10.1021/acsami.1c05833.

[6] H. Kokubo, R. Sano, K. Murai, S. Ishii, and M. Watanabe, "Ionic polymer actuators using poly(ionic liquid) electrolytes," *Eur. Polym. J.*, vol. 106, pp. 266–272, Sep. 2018, doi: 10.1016/j.eurpolymj.2018.07.026.

[7] S. W. Lee *et al.*, "Intrinsically stretchable ionoelastomer junction logic gate synchronously deformable with liquid metal," *Appl. Phys. Rev.*, vol. 9, no. 4, p. 041404, Oct. 2022, doi: 10.1063/5.0104765.

[8] H. J. Kim, B. Chen, Z. Suo, and R. C. Hayward, "Ionoelastomer junctions between polymer networks of fixed anions and cations," *Science*, vol. 367, no. 6479, pp. 773–776, Feb. 2020, doi: 10.1126/science.aay8467.

[9] X. Ming *et al.*, "All-Solid-State Self-Healing Ionic Conductors Enabled by Ion–Dipole Interactions within Fluorinated Poly(Ionic Liquid) Copolymers," *ACS Appl. Mater. Interfaces*, vol. 13, no. 34, pp. 41140–41148, Sep. 2021, doi: 10.1021/acsami.1c12880.

[10] H. Chen, J.-H. Choi, D. Salas-de la Cruz, K. I. Winey, and Y. A. Elabd, "Polymerized Ionic Liquids: The Effect of Random Copolymer Composition on Ion Conduction," *Macromolecules*, vol. 42, no. 13, pp. 4809–4816, Jul. 2009, doi: 10.1021/ma900713e.

[11] A. S. Shaplov *et al.*, "Polymeric Ionic Liquids: Comparison of Polycations and Polyanions," *Macromolecules*, vol. 44, no. 24, pp. 9792–9803, Dec. 2011, doi: 10.1021/ma2014518.

[12] A. S. Shaplov *et al.*, "Design and synthesis of new anionic 'polymeric ionic liquids' with high charge delocalization," *Polym. Chem.*, vol. 2, no. 11, pp. 2609–2618, Oct. 2011, doi: 10.1039/C1PY00282A.

[13] J.-H. Baik, S. Kim, D. G. Hong, and J.-C. Lee, "Gel Polymer Electrolytes Based on Polymerizable Lithium Salt and Poly(ethylene glycol) for Lithium Battery Applications," *ACS Appl. Mater. Interfaces*, vol. 11, no. 33, pp. 29718–29724, Aug. 2019, doi: 10.1021/acsami.9b05139.

[14] C. T. Elmore *et al.*, "Ion Transport in Solvent-Free, Crosslinked, Single-Ion Conducting Polymer Electrolytes for Post-Lithium Ion Batteries," *Batteries*, vol. 4, no. 2, Art. no. 2, Jun. 2018, doi: 10.3390/batteries4020028.

[15] C. Shen, Q. Zhao, N. Shan, B. B. Jing, and C. M. Evans, "Conductivity–modulus–Tg relationships in solvent-free, single lithium ion conducting network electrolytes," *J. Polym. Sci.*, vol. 58, no. 17, pp. 2376–2388, 2020, doi: 10.1002/pol.20200302.

[16] W. Mei, D. Yu, C. George, L. A. Madsen, R. J. Hickey, and R. H. Colby, "Anion chemical composition of poly(ethylene oxide)-based sulfonylimide and sulfonate lithium ionomers controls ion aggregation and conduction," *J. Mater. Chem. C*, vol. 10, no. 39, pp. 14569–14579, 2022, doi: 10.1039/D2TC02212E.

[17] E. I. Lozinskaya *et al.*, "Self-assembly of Li single-ion-conducting block copolymers for improved conductivity and viscoelastic properties," *Electrochimica Acta*, vol. 413, p. 140126, May 2022, doi: 10.1016/j.electacta.2022.140126.

[18] A. Engler, H. Park, N. Liu, and P. A. Kohl, "Dicarbonate acrylate based single-ion conducting polymer electrolytes for lithium batteries," *J. Power Sources*, vol. 574, p. 233145, Aug. 2023, doi:

10.1016/j.jpowsour.2023.233145.
[19] T. N. T. Phan *et al.*, "Vinyl monomers bearing a sulfonyl(trifluoromethane sulfonyl) imide group: synthesis and polymerization using nitroxide-mediated polymerization," *Polym. Chem.*, vol. 7, no. 45, pp. 6901–6910, 2016, doi: 10.1039/C6PY01004K.
[20] G. Luo, B. Yuan, T. Guan, F. Cheng, W. Zhang, and J. Chen, "Synthesis of Single Lithium-Ion Conducting Polymer Electrolyte Membrane for Solid-State Lithium Metal Batteries," *ACS Appl. Energy Mater.*, vol. 2, no. 5, pp. 3028–3034, May 2019, doi: 10.1021/acsaem.9b00440.
[21] M. L. Lehmann, G. Yang, J. Nanda, and T. Saito, "Unraveling Ion Transport in Trifluoromethanesulfonimide Pentablock Copolymer Membranes in Nonaqueous Electrolytes," *Macromolecules*, vol. 55, no. 17, pp. 7740–7751, Sep. 2022, doi: 10.1021/acs.macromol.2c00513.
[22] J. Zhao *et al.*, "Interfacial Polarization and Electroresponsive Electrorheological Effect of Anionic and Cationic Poly(ionic liquids)," *ACS Appl. Polym. Mater.*, vol. 1, no. 11, pp. 2862–2874, Nov. 2019, doi: 10.1021/acsapm.9b00565.
[23] J. Li, H. Zhu, X. Wang, D. R. MacFarlane, M. Armand, and M. Forsyth, "Increased ion conduction in dual cation [sodium][tetraalkylammonium] poly[4-styrenesulfonyl(trifluoromethylsulfonyl)imide-co-ethylacrylate] ionomers," *J. Mater. Chem. A*, vol. 3, no. 39, pp. 19989–19995, Sep. 2015, doi: 10.1039/C5TA04407C.
[24] S. Inceoglu, A. A. Rojas, D. Devaux, X. C. Chen, G. M. Stone, and N. P. Balsara, "Morphology–Conductivity Relationship of Single-Ion-Conducting Block Copolymer Electrolytes for Lithium Batteries," *ACS Macro Lett.*, vol. 3, no. 6, pp. 510–514, Jun. 2014, doi: 10.1021/mz5001948.
[25] C. Ren, M. Liu, J. Zhang, Q. Zhang, X. Zhan, and F. Chen, "Solid-state single-ion conducting comb-like siloxane copolymer electrolyte with improved conductivity and electrochemical window for lithium batteries," *J. Appl. Polym. Sci.*, vol. 135, no. 9, p. 45848, 2018, doi: 10.1002/app.45848.
[26] X. Zhang, B. Guillerm, and R. E. Prud'homme, "Synthesis and thermal properties of a triblock copolymer for lithium metal polymer batteries," *Polymer*, vol. 176, pp. 101–109, Aug. 2019, doi: 10.1016/j.polymer.2019.05.033.
[27] S. D. Jones *et al.*, "Design of Polymeric Zwitterionic Solid Electrolytes with Superionic Lithium Transport," *ACS Cent. Sci.*, vol. 8, no. 2, pp. 169–175, Feb. 2022, doi: 10.1021/acscentsci.1c01260.
[28] J. Liang, K. Xu, S. Arora, J. E. Laaser, and S. K. Fullerton-Shirey, "Ion-Locking in Solid Polymer Electrolytes for Reconfigurable Gateless Lateral Graphene p-n Junctions," *Materials*, vol. 13, no. 5, Art. no. 5, Jan. 2020, doi: 10.3390/ma13051089.
[29] I. Kammakakam, J. E. Bara, E. M. Jackson, J. Lertxundi, D. Mecerreyes, and L. C. Tomé, "Tailored CO2-Philic Anionic Poly(ionic liquid) Composite Membranes: Synthesis, Characterization, and Gas Transport Properties," *ACS Sustain. Chem. Eng.*, vol. 8, no. 15, pp. 5954–5965, Apr. 2020, doi: 10.1021/acssuschemeng.0c00327.
[30] I. Kammakakam, J. E. Bara, and E. M. Jackson, "Dual Anion–Cation Crosslinked Poly(ionic liquid) Composite Membranes for Enhanced CO2 Separation," *ACS Appl. Polym. Mater.*, vol. 2, no. 11, pp. 5067–5076, Nov. 2020, doi: 10.1021/acsapm.0c00877.
[31] J. Liu, P. D. Pickett, B. Park, S. P. Upadhyay, S. V. Orski, and J. L. Schaefer, "Non-solvating, side-chain polymer electrolytes as lithium single-ion conductors: synthesis and ion transport characterization," *Polym. Chem.*, vol. 11, no. 2, pp. 461–471, 2020, doi: 10.1039/C9PY01035A.
[32] H. O. Ford, C. Cui, and J. L. Schaefer, "Comparison of Single-Ion Conducting Polymer Gel Electrolytes for Sodium, Potassium, and Calcium Batteries: Influence of Polymer Chemistry, Cation Identity, Charge Density, and Solvent on Conductivity," *Batteries*, vol. 6, no. 1, Art. no. 1, Mar. 2020, doi: 10.3390/batteries6010011.
[33] J. Dong, L. Krasnova, M. G. Finn, and K. B. Sharpless, "Sulfur(VI) Fluoride Exchange (SuFEx): Another Good Reaction for Click Chemistry," *Angew. Chem. Int. Ed.*, vol. 53, no. 36, pp. 9430–9448, 2014, doi: 10.1002/anie.201309399.
[34] J. W. Wu, R. W. Kulow, M. J. Redding, A. J. Fine, S. M. Grayson, and Q. Michaudel, "Synthesis of Degradable Polysulfamides via Sulfur(VI) Fluoride Exchange Click Polymerization of AB-Type Monomers," *ACS Polym. Au*, vol. 3, no. 3, pp. 259–266, Jun. 2023, doi:

10.1021/acspolymersau.2c00060.
[35] E. M. Thomas, M. K. McBride, O. A. Lee, R. C. Hayward, and A. J. Crosby, "Predicting the Electrical, Mechanical, and Geometric Contributions to Soft Electroadhesives through Fracture Mechanics," *ACS Appl. Mater. Interfaces*, vol. 15, no. 25, pp. 30956–30963, Jun. 2023, doi: 10.1021/acsami.3c03392.
[36] Y. Tao, T. Liu, X. Yang, and J. G. Murphy, "Kinetics and Products of the Aqueous Phase Oxidation of Triethylamine by OH," *ACS Earth Space Chem.*, vol. 5, no. 8, pp. 1889–1895, Aug. 2021, doi: 10.1021/acsearthspacechem.1c00162.
[37] R. Rohan *et al.*, "A high performance polysiloxane-based single ion conducting polymeric electrolyte membrane for application in lithium ion batteries," *J. Mater. Chem. A*, vol. 3, no. 40, pp. 20267–20276, Oct. 2015, doi: 10.1039/C5TA02628H.
[38] C. Yang and Z. Suo, "Hydrogel ionotronics," *Nat. Rev. Mater.*, vol. 3, no. 6, pp. 125–142, Jun. 2018, doi: 10.1038/s41578-018-0018-7.
[39] H.-P. Liang *et al.*, "Polysiloxane-Based Single-Ion Conducting Polymer Blend Electrolyte Comprising Small-Molecule Organic Carbonates for High-Energy and High-Power Lithium-Metal Batteries," *Adv. Energy Mater.*, vol. 12, no. 16, p. 2200013, 2022, doi: 10.1002/aenm.202200013.
[40] M. Alvarez Tirado, L. Castro, G. Guzmán-González, L. Porcarelli, and D. Mecerreyes, "Single- Versus Dual-Ion UV-Cross-Linked Gel Polymer Electrolytes for Li–O2 Batteries," *ACS Appl. Energy Mater.*, vol. 4, no. 1, pp. 295–302, Jan. 2021, doi: 10.1021/acsaem.0c02255.
[41] H.-P. Liang *et al.*, "Photo-Cross-Linked Single-Ion Conducting Polymer Electrolyte for Lithium-Metal Batteries," *Macromol. Rapid Commun.*, vol. 43, no. 12, p. 2100820, 2022, doi: 10.1002/marc.202100820.
[42] G. B. Appetecchi, M. Montanino, M. Carewska, M. Moreno, F. Alessandrini, and S. Passerini, "Chemical–physical properties of bis(perfluoroalkylsulfonyl)imide-based ionic liquids," *Electrochimica Acta*, vol. 56, no. 3, pp. 1300–1307, Jan. 2011, doi: 10.1016/j.electacta.2010.10.023.
[43] P. Kuray *et al.*, "Ion Transport in Pendant and Backbone Polymerized Ionic Liquids," *Macromolecules*, vol. 52, no. 17, pp. 6438–6448, Sep. 2019, doi: 10.1021/acs.macromol.8b02682.
[44] K. Nakamura, T. Saiwaki, K. Fukao, and T. Inoue, "Viscoelastic Behavior of the Polymerized Ionic Liquid Poly(1-ethyl-3-vinylimidazolium bis(trifluoromethanesulfonylimide))," *Macromolecules*, vol. 44, no. 19, pp. 7719–7726, Oct. 2011, doi: 10.1021/ma201611q.
[45] G. J. Tudryn, W. Liu, S.-W. Wang, and R. H. Colby, "Counterion Dynamics in Polyester−Sulfonate Ionomers with Ionic Liquid Counterions," *Macromolecules*, vol. 44, no. 9, pp. 3572–3582, May 2011, doi: 10.1021/ma102547q.
[46] U. H. Choi *et al.*, "Dielectric and Viscoelastic Responses of Imidazolium-Based Ionomers with Different Counterions and Side Chain Lengths," *Macromolecules*, vol. 47, no. 2, pp. 777–790, Jan. 2014, doi: 10.1021/ma402263y.
[47] A. Matsumoto, C. Iacob, T. Noda, O. Urakawa, J. Runt, and T. Inoue, "Introducing Large Counteranions Enhances the Elastic Modulus of Imidazolium-Based Polymerized Ionic Liquids," *Macromolecules*, vol. 51, no. 11, pp. 4129–4142, Jun. 2018, doi: 10.1021/acs.macromol.8b00312.
[48] F. Fan, Y. Wang, T. Hong, M. F. Heres, T. Saito, and A. P. Sokolov, "Ion Conduction in Polymerized Ionic Liquids with Different Pendant Groups," *Macromolecules*, vol. 48, no. 13, pp. 4461–4470, Jul. 2015, doi: 10.1021/acs.macromol.5b00257.
[49] F. Fan *et al.*, "Effect of Molecular Weight on the Ion Transport Mechanism in Polymerized Ionic Liquids," *Macromolecules*, vol. 49, no. 12, pp. 4557–4570, Jun. 2016, doi: 10.1021/acs.macromol.6b00714.
[50] K. Nakamura, K. Fukao, and T. Inoue, "Dielectric Relaxation and Viscoelastic Behavior of Polymerized Ionic Liquids with Various Counteranions," *Macromolecules*, vol. 45, no. 9, pp. 3850–3858, May 2012, doi: 10.1021/ma300040b.
[51] D. S. la Cruz, M. D. Green, Y. Ye, Y. A. Elabd, T. E. Long, and K. I. Winey, "Correlating backbone-to-backbone distance to ionic conductivity in amorphous polymerized ionic liquids," *J. Polym. Sci. Part B Polym. Phys.*, vol. 50, no. 5, pp. 338–346, 2012, doi: 10.1002/polb.23019.

[52] B. Park, H. O. Ford, L. C. Merrill, J. Liu, L. P. Murphy, and J. L. Schaefer, "Dual Cation Exchanged Poly(ionic liquid)s as Magnesium Conducting Electrolytes," *ACS Appl. Polym. Mater.*, vol. 1, no. 11, pp. 2907–2913, Nov. 2019, doi: 10.1021/acsapm.9b00614.
[53] K. Akkaoui, M. Yang, Z. A. Digby, and J. B. Schlenoff, "Ultraviscosity in Entangled Polyelectrolyte Complexes and Coacervates," *Macromolecules*, vol. 53, no. 11, pp. 4234–4246, Jun. 2020, doi: 10.1021/acs.macromol.0c00133.
[54] A. Wulf, K. Fumino, and R. Ludwig, "Spectroscopic Evidence for an Enhanced Anion–Cation Interaction from Hydrogen Bonding in Pure Imidazolium Ionic Liquids," *Angew. Chem. Int. Ed.*, vol. 49, no. 2, pp. 449–453, 2010, doi: 10.1002/anie.200905437.
[55] O. S. Hammond and A.-V. Mudring, "Ionic liquids and deep eutectics as a transformative platform for the synthesis of nanomaterials," *Chem. Commun.*, vol. 58, no. 24, pp. 3865–3892, Mar. 2022, doi: 10.1039/D1CC06543B.
[56] Y. Zhang et al., "Highly Transparent, Underwater Self-Healing, and Ionic Conductive Elastomer Based on Multivalent Ion–Dipole Interactions," Chem. Mater., vol. 32, no. 15, pp. 6310–6317, Aug. 2020, doi: 10.1021/acs.chemmater.0c00096.
[57] S. Huang et al., "Adhering Low Surface Energy Materials without Surface Pretreatment via Ion–Dipole Interactions," ACS Appl. Mater. Interfaces, vol. 13, no. 34, pp. 41112–41119, Sep. 2021, doi: 10.1021/acsami.1c11822.
[58] Y. Umebayashi *et al.*, "Lithium Ion Solvation in Room-Temperature Ionic Liquids Involving Bis(trifluoromethanesulfonyl) Imide Anion Studied by Raman Spectroscopy and DFT Calculations," *J. Phys. Chem. B*, vol. 111, no. 45, pp. 13028–13032, Nov. 2007, doi: 10.1021/jp076869m.
[59] L. C. Loaiza and P. Johansson, "Li-Salt Doped Single-Ion Conducting Polymer Electrolytes for Lithium Battery Application," *Macromol. Chem. Phys.*, vol. 223, no. 8, p. 2100419, 2022, doi: 10.1002/macp.202100419.
[60] E. S. Doyle *et al.*, "Influence of Inorganic Glass Ceramic Particles on Ion States and Ion Transport in Composite Single-Ion Conducting Gel Polymer Electrolytes with Varying Chain Chemistry," *ACS Appl. Polym. Mater.*, vol. 4, no. 2, pp. 1095–1109, Feb. 2022, doi: 10.1021/acsapm.1c01535.

TOC

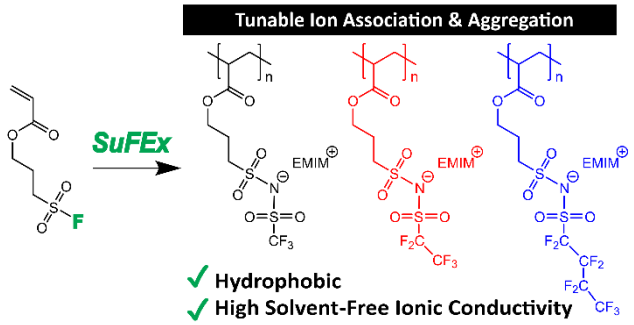
Tunable Ion Association & Aggregation
SuFEx
EMIM
Hydrophobic
High Solvent-Free Ionic Conductivity